

A pulsating white dwarf in an eclipsing binary

Steven G. Parsons^{1,*}, Alexander J. Brown¹, Stuart P. Littlefair¹, Vikram S. Dhillon^{1,2}, Thomas R. Marsh³, J. J. Hermes⁴, Alina G. Istrate⁵, Elmé Breedt⁶, Martin J. Dyer¹, Matthew J. Green³, and David I. Sahman¹

¹Department of Physics & Astronomy, University of Sheffield, Sheffield S3 7RH, UK

²Instituto de Astrofísica de Canarias, Via Lactea s/n, La Laguna, E-38205 Tenerife, Spain

³Department of Physics, Gibbet Hill Road, University of Warwick, Coventry, CV4 7AL, UK

⁴Department of Astronomy, Boston University, 725 Commonwealth Ave. Boston, MA 02215, USA

⁵Department of Astrophysics, Radboud University Nijmegen, P.O. Box 9010, NL-6500 GL Nijmegen, the Netherlands

⁶Institute of Astronomy, University of Cambridge, Madingley Road, Cambridge CB3 0HA, UK

*s.g.parsons@sheffield.ac.uk

ABSTRACT

White dwarfs are the burnt out cores of Sun-like stars and are the final fate of 97% of all stars in our Galaxy. The internal structure and composition of white dwarfs are hidden by their high gravities, which causes all elements, apart from the lightest ones, to settle out of their atmospheres. The most direct method to probe the inner structure of stars and white dwarfs in detail is via asteroseismology. Here we present the first known pulsating white dwarf in an eclipsing binary system, enabling us to place extremely precise constraints on the mass and radius of the white dwarf from the light curve, independent of the pulsations. This $0.325M_{\odot}$ white dwarf — one member of SDSS J115219.99+024814.4 — will serve as a powerful benchmark to constrain empirically the core composition of low-mass stellar remnants and investigate the effects of close binary evolution on the internal structure of white dwarfs.

Introduction

There are thought to be of order 100-300 million close pairs of white dwarfs in the Galaxy^{1,2}. Among these are likely the progenitors of Type Ia supernovae^{3,4}, as well as the progenitors of AM CVn binaries⁵, R CrB stars⁶ and single hot subdwarf stars⁷. Moreover, double white dwarf binaries are expected to be the dominant source of gravitational waves for space-based detectors such as the Laser Interferometer Space Antenna (LISA)^{8,9}. The core composition of white dwarfs in close binaries can have a profound impact on the outcome of their mergers and any resultant supernovae (for example, white dwarfs with oxygen-neon cores are not expected to explode at the Chandrasakar limit but instead will collapse to neutron stars¹⁰), so there is a need to determine interior structures observationally. Some progress has been made recently through precise mass and radius measurements of white dwarfs in eclipsing binaries¹¹, but ultimately it is asteroseismology that offers the best probe of white dwarf interiors¹²⁻¹⁴, capable for example of constraining the carbon/oxygen ratio in white dwarf cores¹⁵ and of measuring helium and hydrogen layer masses¹⁶. Asteroseismology is also the most definitive way to test for the existence of “hybrid”-core white dwarfs (carbon-oxygen cores but up to 25 per cent helium by mass), where the distinction from standard carbon-oxygen core white dwarfs is rather subtle¹⁷.

Helium-core, low-mass carbon-oxygen and hybrid core white dwarfs are all expected to be particularly prevalent amongst the low mass white dwarf products of binary evolution¹⁷, making pulsating white dwarfs in binaries with masses in the range 0.3 to $0.5M_{\odot}$ of particular interest. Amongst the ~ 300 known pulsating white dwarfs¹⁸, very few are in binaries. In fact, apart from a handful of unusual and extremely low mass ($< 0.2M_{\odot}$) white dwarf pulsators^{19,20}, there is only one known pulsating white dwarf in a detached binary²¹, and at $0.6M_{\odot}$ it is almost certainly a standard carbon-oxygen core white dwarf²².

In this paper we report the discovery of pulsations from the cooler component of the eclipsing double white dwarf binary SDSS J115219.99+024814.4 (hereafter SDSS J1152+0248), making it the first known pulsating white dwarf in an eclipsing binary. SDSS J1152+0248 is a 2.4 hour binary consisting of two low-mass white dwarfs discovered using data from the *Kepler* K2 mission²³. Preliminary estimates of the parameters of the white dwarfs implied that the cooler component may be close to the ZZ Ceti instability strip²³, but these estimates were highly uncertain due to the fact that only one white dwarf (the hotter) could be seen spectroscopically (i.e. the system appeared single-lined). The higher-quality data presented in this paper unambiguously reveal the system as double-lined, allowing us to measure both masses directly. Moreover, our high time-resolution light curves reveal pulsations from the cooler white dwarf with at least three significant periods (1314, 1069

and 583 seconds) and allow us to constrain the radii of both white dwarfs to high precision (by modelling the eclipse profiles), independent of any theoretical models. Both white dwarfs may have either helium or hybrid helium-carbon-oxygen cores.

Results

Following the discovery of SDSS J1152+0248 we obtained time-series spectroscopy of the system with the X-shooter echelle spectrograph²⁴ on the 8.2 m Very Large Telescope, with the aim of detecting the cooler white dwarf and measuring the radial velocity curves of both components. In addition to this, we obtained 108 minutes of high-speed photometry of the binary using HiPERCAM²⁵ on the 10.4 m Gran Telescopio Canarias, which revealed not only the primary and secondary eclipses but also pulsations from the cooler component. Combining both these data sets allows us to measure the stellar and binary parameters of SDSS J1152+0248, which are provided in Table 1.

Parameter	units	value	uncertainty
Orbital period	days	0.099 865 265 42	$\pm 0.000\,000\,000\,10$
Centre of WD ₁ eclipse	MJD(BTDB)	57460.651 021 8	$\pm 0.000\,001\,0$
K_1	km s^{-1}	190.6	± 1.5
K_2	km s^{-1}	212.3	± 10.5
γ_1	km s^{-1}	60.2	± 1.0
γ_2	km s^{-1}	55.7	± 7.2
<i>Gaia</i> parallax ²⁶	mas	1.40	± 0.26
Bayesian distance ²⁷	pc	706	-119 +175
Right ascension	deg (J2000)	178.08337	
Declination	deg (J2000)	2.80399	
SDSS g	mag	18.32	± 0.01
Binary inclination	degrees	89.44	-0.03 +0.04
Binary separation	R_\odot	0.799	± 0.010
Mass ratio	M_1 / M_2	1.11	± 0.025
M_1	M_\odot	0.362	± 0.014
M_2	M_\odot	0.325	± 0.013
R_1	R_\odot	0.0212	± 0.0003
R_2	R_\odot	0.0191	± 0.0004
$\log g_1$	dex	7.344	± 0.014
$\log g_2$	dex	7.386	± 0.012
$T_{\text{eff},1}$ (eclipse)	K	20800	-960 +1060
$T_{\text{eff},1}$ (SED)	K	21200	-1100 +1200
$T_{\text{eff},2}$ (eclipse)	K	10400	-340 +400
$T_{\text{eff},2}$ (SED)	K	11100	-770 +950
$E(B-V)$	mag	0.07	± 0.02

Table 1. Stellar and binary parameters for SDSS J1152+0248. The subscript 1 refers to the brighter, hotter, more massive white dwarf, while 2 refers to the fainter, cooler white dwarf, which is the pulsator. We list the effective temperatures for each white dwarf as determined from both the eclipse light curves and the spectral energy distribution fit. The ephemeris values were derived from a combination of our light curve fit and previous measurements²³. Quoted uncertainties represent the one-sigma confidence intervals.

The radial velocity semi-amplitudes of both white dwarfs

The radial velocity semi-amplitudes for both white dwarfs were determined by fitting the $H\alpha$ absorption line, specifically the narrow non-LTE core of the line. On first inspection the line from the fainter white dwarf is not obvious in the data (the left-hand panel of Figure 1), given that it only contributes $\sim 20\%$ of the light at this wavelength. However, when a good model for the brighter component is subtracted then the absorption from the fainter white dwarf is seen moving in anti-phase (the third panel of Figure 1). We therefore fitted the X-shooter data with components from both white dwarfs (see the Methods section for a full description of the procedure). We calculated the orbital phase of each spectrum using the ephemeris determined from our light curve fitting (see the next section) and then fitted all spectra simultaneously, shifting the absorption components according to the orbital phase. This approach is useful for determining the velocity of the fainter component, which is often

difficult to fit in an individual spectrum. The best fit model is shown in the second panel of Figure 1 and the residual of the fit in the right-most panel. The radial velocity values are listed in Table 1 and indicate a binary mass ratio close to unity.

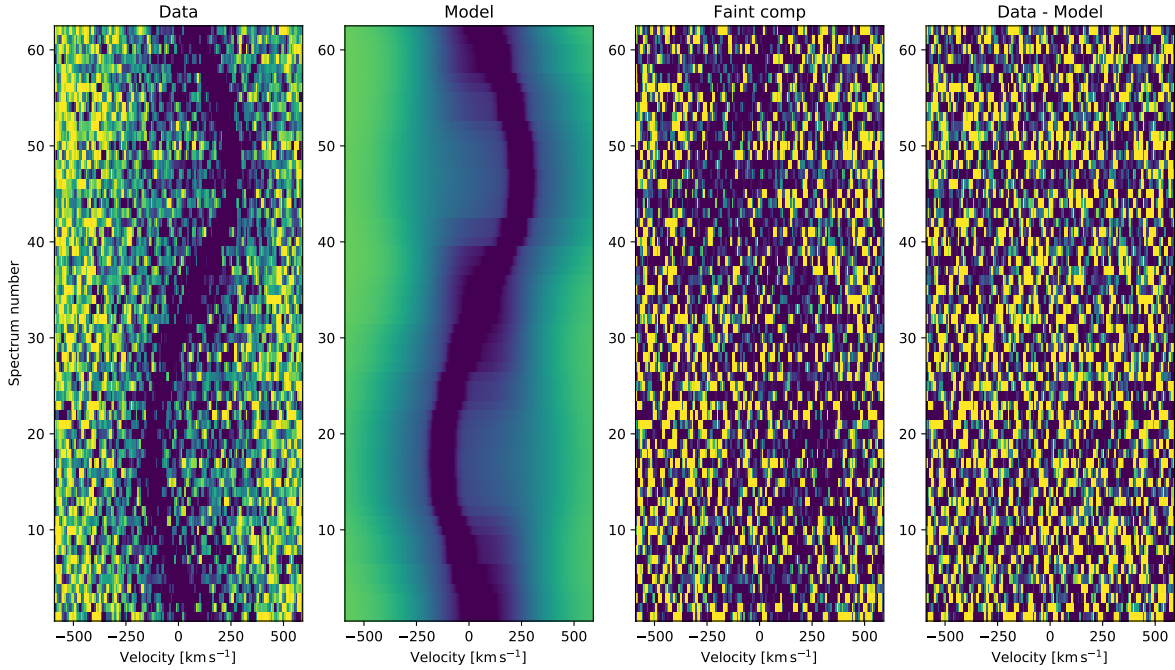


Figure 1. Triled spectrogram of the $H\alpha$ line of SDSS J1152+0248. The left-most panel shows the X-shooter data, where the spectra have been ordered in ascending orbital phase (starting and ending at phase 0). The strong absorption line from the hot white dwarf is clearly evident. The next panel shows our best fit model, which includes components from both white dwarfs. The third panel shows the X-shooter data after subtracting the best fit model with only the brighter component included (i.e. it shows only the data for the fainter component). The right-most panel shows the residuals to the fit after including the fainter component as well. The colour scale in the two right-hand plots has been stretched using a sinh stretch to emphasise the lower fluxes of the absorption line from the fainter white dwarf.

The masses, radii and effective temperatures of both white dwarfs

The high-speed HiPERCAM light curves of SDSS J1152+0248 (Figure 2) reveal both the primary eclipse (the eclipse of the hotter white dwarf at phase 1.0) and the secondary eclipse (the eclipse of the fainter white dwarf at phase 0.5). Combined with the radial-velocity data from the X-shooter spectroscopy, the light curves allow us to measure the masses and radii of both white dwarfs directly, virtually independent of theoretical models. Moreover, the multi-band light curve data (covering the entire optical wavelength range) also constrains the effective temperatures of the two white dwarfs via the differences in eclipse depths in the different bands.

We used `LCURVE`²⁸ to fit the HiPERCAM data of SDSS J1152+0248, which is a code designed to fit the light curves of white dwarf binaries (see the methods section for full details of the light curve fitting procedure). Note that although the pulsations from the cooler white dwarf are not visible in Figure 2 (due to the plot scale), they are sufficiently large (see the next section) that they needed to be taken into account when fitting the light curves or they would have resulted in systematic errors on the final fit parameters. Therefore, we modelled the pulsations using Gaussian Processes²⁹, which are ideal for modelling periodic signals that are not exactly sinusoidal (see the methods section for more details). The derived parameters from the light curve fit and their errors are listed in Table 1. The best fit models are shown in Figure 2. The measured mass of the cooler white dwarf is lower than in the discovery paper²³ due to an overestimation of the temperatures of the two white dwarfs in that paper. More reliable temperature estimates were only possible due to the combination of our direct detection of the lines from the cooler white dwarf and our multi-band photometric data.

In addition to the light curve fit we also constrained the temperatures of the two white dwarfs by fitting the spectral energy distribution (SED) of SDSS J1152+0248. We retrieved archival photometry from GALEX (FUV and NUV bands), SDSS (*ugriz* bands) and UKIDSS (*YJH* bands) and fitted these data with a combination of two DA white dwarf spectra³⁰ with the same brightness ratios as measured from the HiPERCAM light curves (see the methods section for details of this fit). The result is

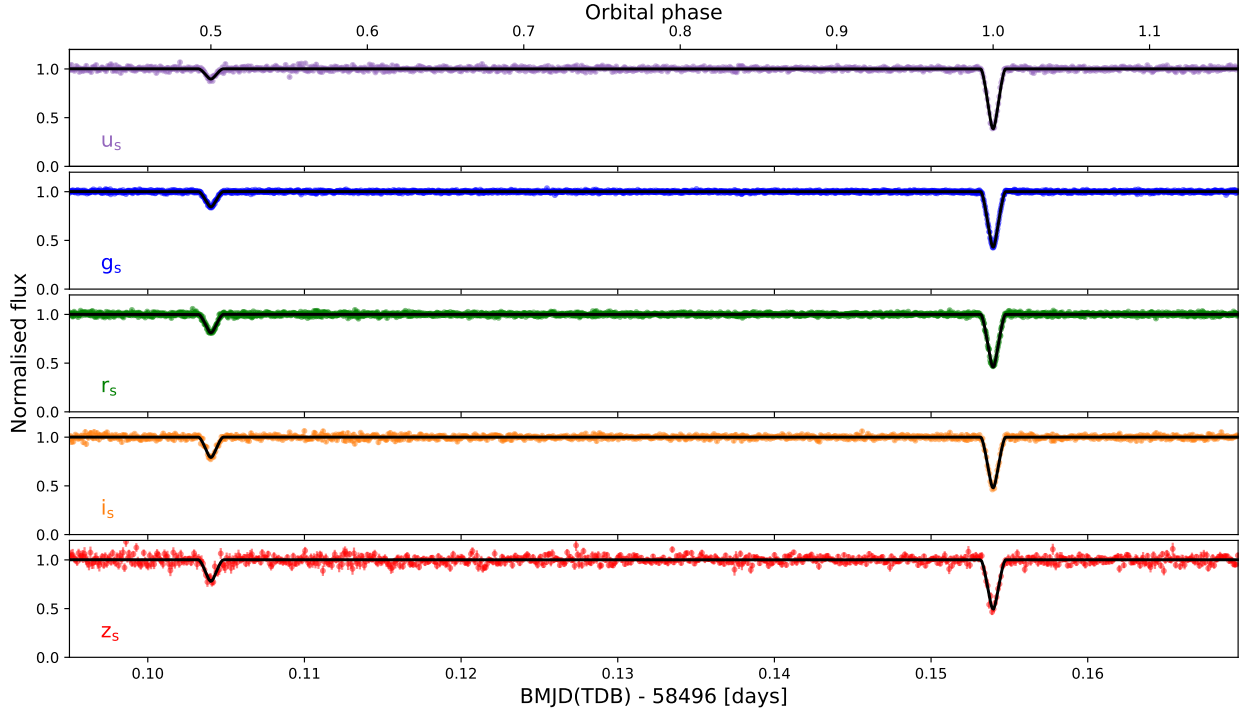


Figure 2. HiPERCAM high-speed light curves of SDSS J1152+0248 with model fits overplotted. The eclipse of the fainter (cooler) white dwarf occurs at phase 0.5, while the eclipse of the brighter (hotter) white dwarf occurs at phase 1.0. The pulsations from the fainter white dwarf are not visible at this scale.

shown in Figure 3 and gives temperatures consistent with the fit to the multi-band eclipse light curves.

The pulsations of the cool white dwarf

The HiPERCAM light curves show small scale periodic variations most easily seen in the g_s band (see the left-hand panel of Figure 4). A periodogram³¹ of the data (with the eclipses removed using the binary light curve solution) reveals a strong peak at a frequency of 0.76 mHz, corresponding to a period of 1314.0 ± 5.9 seconds (the right-hand panel of Figure 4), which is seen in all bands, although the detection is only marginal in the z_s band. There are also other peaks at frequencies of 0.96 mHz (period of 1069.0 ± 12.5 seconds, which is detected in the g_s band and marginally in the r_s band) and at 1.71 mHz (period of 583.4 ± 4.3 seconds, detected only in the g_s band). These pulsations are in line for those expected for non-radial g -mode pulsations of a $\sim 0.3 M_\odot$ white dwarf¹⁹. The short baseline of the HiPERCAM observations makes a more detailed asteroseismic analysis impossible at this time.

With a mass of $0.325 \pm 0.013 M_\odot$ the pulsating white dwarf in SDSS J1152+0248 sits in a poorly sampled region of the ZZ Ceti instability strip between standard carbon-oxygen core ZZ Ceti white dwarfs and the extremely low-mass helium-core pulsators³².

Discussion

The measured masses and radii of the white dwarfs in SDSS J1152+0248 are virtually model-independent (there is some small dependence upon the adopted limb darkening parameters, but this is at a level smaller than the final quoted uncertainties) and as such, comparing them to theoretical mass-radius relationships can offer insight into their internal composition¹¹. Figure 5 shows the measured parameters of both white dwarfs in SDSS J1152+0248 compared to theoretical models of white dwarfs with different core compositions and surface hydrogen layer thicknesses. Given the low masses of both white dwarfs ($0.36 M_\odot$ and $0.33 M_\odot$) we would expect them to have helium cores³⁶; for example, this is the case for the similar eclipsing double white dwarf system CSS 41177^{37,38}. However, the measured radii of both white dwarfs are too small to be consistent with pure helium core models (both white dwarfs have measured radii approximately 10% smaller than helium core models would predict³³). On the contrary, they are more consistent with carbon-oxygen cores. While there are predictions that carbon-oxygen core white dwarfs can form at masses as low as $0.33 M_\odot$ ³⁹, it requires substantial mass loss along the red giant branch⁴⁰. In order

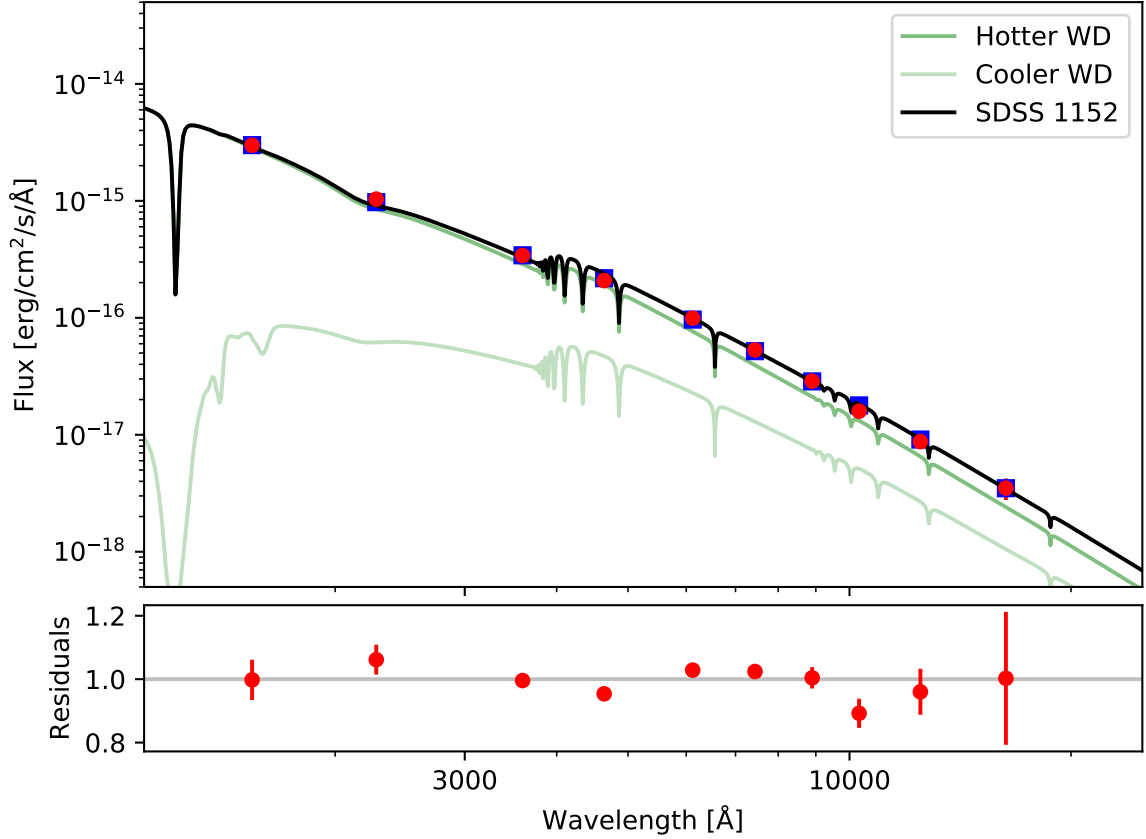


Figure 3. Spectral energy distribution of SDSS J1152+0248 (red points are GALEX, SDSS and UKIDSS measurements) with best fit model spectrum (black line and blue squares). The model spectrum is a combination of two white dwarf models (individual components shown in green) that have been scaled to match the contribution of each white dwarf in the optical based on the fits to the HiPERCAM eclipse light curves. The lower panel shows the residuals to the fit.

to have carbon-oxygen cores at such low masses, these white dwarfs would have needed to be initially quite massive stars ($\gtrsim 2.3 M_{\odot}$), since they would have avoided the helium flash (as their evolution was cut short before the end of the red giant branch). This would make the system quite young as the main-sequence lifetimes of such stars is only ~ 1 Gyr. However, the tangential velocity of SDSS J1152+0248 from *Gaia* DR2 is more than 120 km s^{-1} . This, combined with the large systemic velocity measured from the X-shooter data (55 km s^{-1}) implies that the system is much older than this⁴¹.

Alternatively, the white dwarfs in SDSS J1152+0248 may have hybrid helium-carbon-oxygen cores, which have radii similar to carbon-oxygen core white dwarfs¹⁷. It is also possible that these are helium-core white dwarfs with extremely thin surface hydrogen layers ($M_H/M_* < 10^{-8}$), although producing such a thin surface layer is difficult³³. The mass-radius measurements alone cannot distinguish between these two possibilities (helium-cores with thin surface hydrogen layers or hybrid helium-carbon-oxygen cores), however, the pulsations from the cooler white dwarf may be able to distinguish between these scenarios in the future. In particular, the mean period spacing (the period between consecutive radial overtones of a given spherical degree) will be different for alternative core compositions and is likely to be the definitive test, but this requires substantially more data than the short HiPERCAM light curve presented here. A full asteroseismic analysis, combined with the binary analysis presented in this paper, would allow us to probe the internal structure of a white dwarf that has experienced several episodes of past mass transfer within a binary system. SDSS J1152+0248 is therefore an ideal system for investigating how binary interactions affect the structure of white dwarfs.

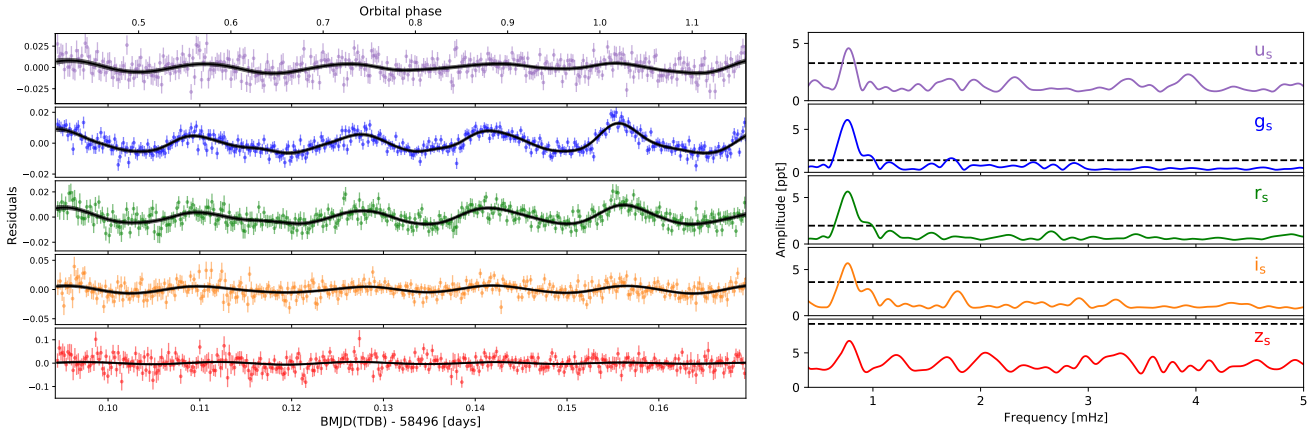


Figure 4. The pulsations of the cool white dwarf in SDSS J1152+0248. *Left:* HiPERCAM light curve residuals after subtraction of the binary model in u_s , g_s , r_s , i_s , z_s , respectively. The data have been binned in time by a factor of 5 for clarity. The pulsations are most evident in the g_s band data. Overplotted is the best fit Gaussian Process model that was used to account for the pulsations when fitting the light curve. *Right:* Periodograms of the residual light curves showing a clear peak at a frequency of 0.76mHz (period of 1314 seconds), with additional peaks at 0.94mHz (period of 1059 seconds, significant in the g_s and r_s bands) and at 1.71mHz (period of 583 seconds, significant only in the g_s band). The horizontal dashed lines show the 1% false-alarm probabilities in each band (see the methods section for details of how these were calculated).

Methods

Observations and their reduction

SDSS J1152+0248 was observed with the medium resolution echelle spectrograph X-shooter²⁴ on the 8.2m Very Large Telescope (VLT) in Chile. Observations were performed in service mode covering one full orbit of the binary each time on 4 separate nights (March 4 2017, May 18 2017, January 17 2018 and January 20 2018). X-shooter covers a wavelength range from the UV cutoff in the blue (3000Å) to the edge of the K -band in the red (2.5 microns) in three separate arms, the UVB (3000-5600Å), VIS (5600-10100Å) and NIR arms (10100-25000Å). We used slit widths of 1" in the UVB arm and 0.9" in the VIS and NIR arms and binned by a factor of 2 in the spatial direction in the UVB and VIS arms, resulting in a resolution of ~ 7500 . To mitigate the effects of orbital smearing we kept exposure times short (565, 555s, 600 seconds in the UVB, VIS and NIR arms respectively). Due to the faintness of SDSS J1152+0248 in the NIR ($J = 18.8$) these spectra have very low signal-to-noise and were therefore not used in any subsequent analysis. The data were reduced using the latest release of the X-Shooter reduction pipeline (version 3.2.0) using standard reduction steps. All spectra were placed on a barycentric wavelength scale.

Multi-band photometry of SDSS J1152+0248 was obtained with HiPERCAM²⁵ mounted on the 10.4m Gran Telescopio Canarias (GTC) on the 12th of January 2019. HiPERCAM is a high-speed quintuple-beam imager capable of obtaining simultaneous u , g , r , i and z band imaging at frames rates of up to 1000 frames per second with a dead time of only 0.01 seconds between exposures. HiPERCAM uses modified versions of the Sloan filters with much higher throughput, known as Super-SDSS filters. These are denoted as u_s, g_s, r_s, i_s, z_s to distinguish them from the standard SDSS filters ($ugriz$). HiPERCAM allows exposure times to differ for each band, but must remain integer values of each other. Therefore, for SDSS J1152+0248 we used an exposure time of 2.7 seconds in the g_s and r_s bands, 5.4 seconds in the u_s and i_s bands and 8.1 seconds in the z_s band, resulting in a signal-to-noise ratio of 100-200 per frame. We recorded a total of 108 minutes of data covering both a primary and secondary eclipse as well as a substantial amount of out-of-eclipse data. The data were reduced using the HiPERCAM pipeline, including fringe correction in the z_s band. Differential photometry was performed using the nearby star SDSS J115222.49+024931.1 as a reference source. Note that this source is listed as an RR Lyrae star in SIMBAD, but we see no clear variability of this source during our ~ 2 hour observations. An additional source, SDSS J115220.95+024828.4, was used as a check star to confirm the lack of variability of the comparison star. All times were converted to the barycentric dynamical timescale, corrected to the solar system barycentre, BMJD(TDB).

The radial velocity fitting method

In order to measure the radial velocity semi-amplitudes of both white dwarfs in SDSS J1152+0248 we fitted the $H\alpha$ absorption line, where both components are visible (see Figure 1). The spectra were first continuum normalised by fitting a first-order

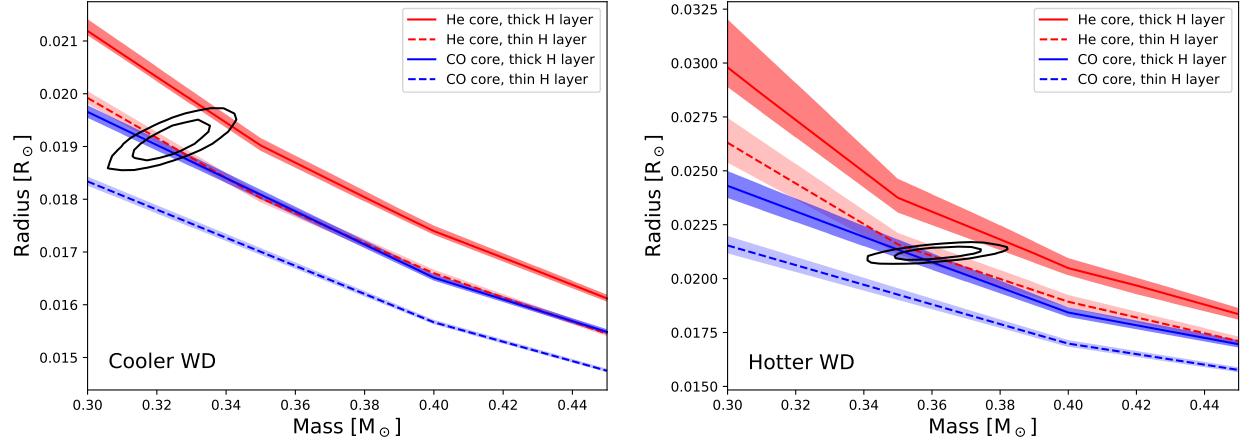


Figure 5. Constraints on the masses and radii of the white dwarfs in SDSS J1152+0248 shown as contours (68 and 95 percentile regions). Also plotted are theoretical models for helium core white dwarfs with thick³³ ($M_H/M_* = 10^{-3}$) and thin³⁴ ($M_H/M_* = 10^{-8}$) surface hydrogen layers and carbon-oxygen core white dwarfs with thick ($M_H/M_* = 10^{-4}$) and thin ($M_H/M_* = 10^{-10}$) surface hydrogen layers³⁵. The theoretical models have the same temperatures as the white dwarfs in SDSS J1152+0248 (the shaded regions account for the uncertainty in the measured temperatures). It is also possible that these are both hybrid helium-carbon-oxygen core white dwarfs (which sit between the different models¹⁷).

polynomial to a small region either side of the $H\alpha$ line (from -2000 km s^{-1} to -1000 km s^{-1} and $+1000 \text{ km s}^{-1}$ to $+2000 \text{ km s}^{-1}$). We then fitted the $H\alpha$ line (from -600 km s^{-1} to $+600 \text{ km s}^{-1}$, hence far from the Lorentzian wings of the line) in all 62 spectra simultaneously using a combination of a first-order polynomial and three Gaussian components. We modelled the brighter white dwarf’s absorption with two Gaussians, one representing the narrow non-LTE core of the line, while the other represents the broader absorption component. The non-LTE core of the $H\alpha$ line can be well approximated by a Gaussian. The fainter white dwarf was modelled with a single Gaussian component. The amplitude (A) and width (σ) of each Gaussian component was the same in all spectra, but their velocities (V) were allowed to vary from spectrum to spectrum, based on the orbital phase (ϕ):

$$V_{1,2} = \gamma_{1,2} + K_{1,2} \sin 2\pi\phi, \quad (1)$$

where γ is the systemic velocity and K is the radial velocity semi-amplitude (the subscript 1 and 2 refer to the brighter and fainter white dwarfs respectively). The two Gaussian components representing the brighter white dwarf were forced to share the same values of γ_1 and K_1 .

The distributions of our model parameters were found using the Markov chain Monte Carlo (MCMC) method⁴² implemented using the python package EMCEE⁴³, where the likelihood of accepting a model was based on the χ^2 of the fit. A short initial MCMC chain was used to determine the approximate parameters values, which were then used as the starting values in a longer “production” chain, to determine the final values and their uncertainties. The production chain used 50 walkers, each with 6,000 points. The first 1,000 points were classified as “burn-in” and were removed from the final results. The final parameters distributions are shown in Supplementary Figure 1.

The light curve fitting method

The HiPERCAM eclipse light curves are sensitive to the radii of the two white dwarfs, the orbital inclination and (due to the multi-band nature of HiPERCAM) also the temperatures of both white dwarfs. We generated model light curves of the system using LCURVE²⁸, which includes the effects of eclipses, Roche geometry distortion and limb- and gravity-darkening. Additionally, the code includes irradiation but this is negligible in SDSS J1152+0248 and so it was ignored in our modelling. LCURVE sets the surface brightnesses of the white dwarfs assuming a black body of a given temperature. However, white dwarf spectral energy distributions can depart substantially from a black body and therefore the temperatures returned by LCURVE do not accurately reflect the effective temperatures of the white dwarfs. To overcome this we computed black body temperatures for a wide range of white dwarf parameters in the *ugriz* bands from cooling models^{44,45}, in this way we could input a single effective temperature and surface gravity for each white dwarf and convert these into black body temperatures for each band before computing the light curve model.

We used the four-parameter non-linear limb darkening model⁴⁶, which takes the form

$$\frac{I(\mu)}{I(1)} = 1 - \sum_{k=1}^4 a_k (1 - \mu^{\frac{k}{2}}), \quad (2)$$

where $\mu = \cos \phi$ (ϕ is the angle between the line of sight and the emergent flux), a_k are the limb darkening coefficients and $I(1)$ is the monochromatic specific intensity at the centre of the stellar disk. Coefficients for both white dwarfs were interpolated from tabulated values⁴⁷.

The input parameters to our light curve model were the mid-time of the primary (deeper) eclipse T_0 , the orbital period of the binary P_{orb} , the binary inclination i , the effective temperatures of both white dwarfs T_{eff} , and their masses (M) and radii (R), from which we calculate their surface gravities and thus limb-darkening coefficients and black body temperatures for each band. We also calculated the orbital separation a , since LCURVE takes scaled radii (R/a) as input parameters, rather than physical radii.

In addition to these stellar and binary parameters we also simultaneously modelled the pulsations from the cooler white dwarf with a Gaussian Process regression model implemented using the Python package CELERITE⁴⁸. Gaussian process models parametrize the covariance between data points by means of a kernel function. We used a damped harmonic oscillator kernel to represent the periodic variations caused by the pulsations of the white dwarf. The kernel is defined by three parameters, the amplitude (pulse_amp), frequency (pulse_omega) and quality factor (pulse_q). These parameters are fixed between the different HiPERCAM bands, but the amplitude is then re-scaled in each band based on a black body temperature (pulse_temp).

Model parameters and their uncertainties were found using the MCMC method. However, unlike the radial velocity fitting, in this case the likelihood of accepting a model was based on a combination of the χ^2 of the fit to the light curve data and an additional prior probability to ensure that the masses were consistent with the measured radial velocities. Moreover, the previous eclipse timing data²³ were included to improve the accuracy and precision of the ephemeris. As before, initial chains were used to determine the starting parameters for a full production chain. This final chain contained 50,000 points, of which the first 5,000 were excluded as burn-in. The final parameters distributions are shown in Supplementary Figure 2.

While our results are generally in agreement with the original study of this system²³, the temperatures for both white dwarfs are significantly lower, as is the mass of the cooler component. All of these discrepancies are due to an overestimation of the contribution from the cooler component in the original study. In the original study the cooler component was found to contribute 31% of the total g band flux. Our higher quality data shows that its contribution is 22.4% in the g band. Their higher contribution was then folded into the analysis of the spectral energy distribution in the original study, resulting in an overestimation of the temperatures of both white dwarfs. This was compounded by the lack of *Gaia* data to constrain the distance and the fact that they only had eclipse data in a single photometric band. In the original study the mass of the cooler white dwarf was then determined using a mass-radius relationship for a fixed temperature. However, as this temperature was too high it caused an overestimation of the mass (since at a fixed temperature higher mass white dwarfs have smaller radii). Lower mass white dwarfs were excluded since their radii would have been too large at these hotter temperatures. However, the methodology used in that study is still sound; had they used the temperatures that we measured then their analysis would have yielded a similar mass for the cooler white dwarf (since a 10,500 K 0.33 M_{\odot} white dwarf has a similar radius to a 14,500 K 0.44 M_{\odot} white dwarf).

The spectral energy distribution fitting method

In addition to constraining the temperatures of both white dwarfs via the multi-band eclipse light curves, we also performed a fit to the spectral energy distribution of SDSS J1152+0248 in order to measure independently the temperatures via this method. We fitted the GALEX, SDSS and UKIDSS photometry with a combination of two model DA white dwarf spectra³⁰. The input parameters for the fit were the temperatures and surface gravities of both white dwarfs and the parallax and reddening $E(B - V)$, of the system. The model spectra for each white dwarf were scaled to the distance implied from the parallax (by simple parallax inversion and using a mass-radius relationship³⁵), reddened, and combined. Model parameters and their uncertainties were again found using the MCMC method. We included an additional prior probability based on the *Gaia* parallax²⁶ and set an upper limit on the reddening of $E(B - V) < 0.106$ based on reddening maps⁴⁹. Our prior also ensured that the masses were consistent with the spectroscopic values and that the relative contribution of each white dwarf in the SDSS *ugriz* bands were consistent with the measurements from the eclipse light curves. We again used initial chains to determine the starting parameters for the final production chains. The final chain contained 10,000 points and the first 2,000 were excluded as burn-in. The final parameters distributions are shown in Supplementary Figure 3.

Pulsation analysis

We explored possible oscillation frequencies of the binary-light-curve-model-subtracted residuals using the PERIOD04 software package⁵⁰. For each of the five bandpasses we determined what signals in the periodogram were significant by determining

a 1% false-alarm probability. To do so we kept the time sampling of the light curve the same but randomly shuffled the flux values 10,000 times, taking the top 1% of the cumulative distribution of highest peaks from each synthetic, shuffled light curve as the 1% false-alarm probability⁵¹. The 1% false-alarm probabilities are shown in Figure 4 (u_s : 3.28 ppt (parts per thousand); g_s : 1.41 ppt; r_s : 1.97 ppt; i_s : 3.64 ppt; z_s : 9.20 ppt), and we consider any peaks in the periodogram above these values to be significant. One significant signal is detected in u_s at 1300 ± 18 s (42.9 ± 5.4 ppt amplitude). Three significant signals are detected in g_s at 1314.0 ± 5.9 s (33.0 ± 1.3 ppt amplitude), 1059 ± 13 s (9.8 ± 1.3 ppt amplitude), and 582.9 ± 4.3 s (8.9 ± 1.3 ppt amplitude). Two significant signals are present in r_s at 1319.4 ± 9.5 s (25.3 ± 1.6 ppt amplitude) and 1050 ± 17 s (9.1 ± 1.6 ppt amplitude). One significant signal is present in i_s at 1320 ± 19 s (22.7 ± 2.9 ppt amplitude). There are no significant signals in z_s . The reported pulsation amplitudes have been adjusted from those measured and shown in Figure 4 to account for the flux contribution of the pulsating secondary white dwarf in each bandpass (u_s : $12.3 \pm 0.5\%$; g_s : $18.4 \pm 0.2\%$; r_s : $22.4 \pm 0.2\%$; i_s : $24.8 \pm 0.2\%$; z_s : $26.4 \pm 0.3\%$). We have adopted the pulsation periods determined from the g_s in the manuscript, since they have the highest signal-to-noise.

Data availability

The raw and reduced X-shooter data presented in this paper are available from the ESO archive: <http://archive.eso.org/cms.html>. Raw and reduced HiPERCAM data are available from the GTC archive: <http://gtc.sdc.cab.inta-csic.es/gtc/index.jsp>. These data can also be obtained from the corresponding author upon reasonable request.

Code availability

The X-Shooter reduction pipeline (version 3.2.0) is available at <https://www.eso.org/sci/software/pipelines/xshooter/> and the HiPERCAM pipeline at <https://github.com/HiPERCAM/hipercam>. The light-curve fitting method is available at <https://github.com/trmrsh/cpp-lcurve>. The codes used to generate the plots presented in this paper are available from the corresponding author upon reasonable request.

References

1. Maxted, P. F. L. & Marsh, T. R. The fraction of double degenerates among DA white dwarfs. *Mon. Not. R. Astron. Soc.* **307**, 122–132, DOI: [10.1046/j.1365-8711.1999.02635.x](https://doi.org/10.1046/j.1365-8711.1999.02635.x) (1999). [astro-ph/9901273](https://arxiv.org/abs/astro-ph/9901273).
2. Nelemans, G., Yungelson, L. R. & Portegies Zwart, S. F. The gravitational wave signal from the Galactic disk population of binaries containing two compact objects. *Astron. Astrophys.* **375**, 890–898, DOI: [10.1051/0004-6361/20010683](https://doi.org/10.1051/0004-6361/20010683) (2001). [astro-ph/0105221](https://arxiv.org/abs/astro-ph/0105221).
3. Tutukov, A. V. & Yungelson, L. R. On the influence of emission of gravitational waves on the evolution of low-mass close binary stars. *Acta Astron.* **29**, 665–680 (1979).
4. Webbink, R. F. Double white dwarfs as progenitors of R Coronae Borealis stars and Type I supernovae. *Astrophys. J.* **277**, 355–360, DOI: [10.1086/161701](https://doi.org/10.1086/161701) (1984).
5. Paczyński, B. Gravitational Waves and the Evolution of Close Binaries. *Acta Astron.* **17**, 287 (1967).
6. Iben, J., Icko, Tutukov, A. V. & Yungelson, L. R. On the Origin of Hydrogen-deficient Supergiants and Their Relation to R Coronae Borealis Stars and Non-DA White Dwarfs. *Astrophys. J.* **456**, 750, DOI: [10.1086/176694](https://doi.org/10.1086/176694) (1996).
7. Han, Z., Podsiadlowski, P., Maxted, P. F. L. & Marsh, T. R. The origin of subdwarf B stars - II. *Mon. Not. R. Astron. Soc.* **341**, 669–691, DOI: [10.1046/j.1365-8711.2003.06451.x](https://doi.org/10.1046/j.1365-8711.2003.06451.x) (2003). [astro-ph/0301380](https://arxiv.org/abs/astro-ph/0301380).
8. Nelemans, G. The Galactic gravitational wave foreground. *Class. Quantum Gravity* **26**, 094030, DOI: [10.1088/0264-9381/26/9/094030](https://doi.org/10.1088/0264-9381/26/9/094030) (2009). [0901.1778](https://arxiv.org/abs/0901.1778).
9. Marsh, T. R. Double white dwarfs and LISA. *Class. Quantum Gravity* **28**, 094019, DOI: [10.1088/0264-9381/28/9/094019](https://doi.org/10.1088/0264-9381/28/9/094019) (2011). [1101.4970](https://arxiv.org/abs/1101.4970).
10. Nomoto, K. & Kondo, Y. Conditions for accretion-induced collapse of white dwarfs. *Astrophys. J. Lett.* **367**, L19–L22, DOI: [10.1086/185922](https://doi.org/10.1086/185922) (1991).
11. Parsons, S. G. *et al.* Testing the white dwarf mass-radius relationship with eclipsing binaries. *Mon. Not. R. Astron. Soc.* **470**, 4473–4492, DOI: [10.1093/mnras/stx1522](https://doi.org/10.1093/mnras/stx1522) (2017). [1706.05016](https://arxiv.org/abs/1706.05016).
12. Fontaine, G. & Brassard, P. The Pulsating White Dwarf Stars. *Publ. Astron. Soc. Pac.* **120**, 1043, DOI: [10.1086/592788](https://doi.org/10.1086/592788) (2008).

13. Winget, D. E. & Kepler, S. O. Pulsating white dwarf stars and precision asteroseismology. *Annu. Rev. Astron. Astrophys.* **46**, 157–199, DOI: [10.1146/annurev.astro.46.060407.145250](https://doi.org/10.1146/annurev.astro.46.060407.145250) (2008). [0806.2573](https://doi.org/10.1146/annurev.astro.46.060407.145250).
14. Althaus, L. G., Córscico, A. H., Isern, J. & García-Berro, E. Evolutionary and pulsational properties of white dwarf stars. *Astron. Astrophys. Rev.* **18**, 471–566, DOI: [10.1007/s00159-010-0033-1](https://doi.org/10.1007/s00159-010-0033-1) (2010). [1007.2659](https://doi.org/10.1007/s00159-010-0033-1).
15. Charpinet, S., Brassard, P., Giammichele, N. & Fontaine, G. Improved seismic model of the pulsating DB white dwarf KIC 08626021 corrected from the effects of neutrino cooling. *Astron. Astrophys.* **628**, L2, DOI: [10.1051/0004-6361/201935823](https://doi.org/10.1051/0004-6361/201935823) (2019).
16. Clemens, J. C., O’Brien, P. C., Dunlap, B. H. & Hermes, J. J. Seismology of an Ensemble of ZZ Ceti Stars. In Tremblay, P. E., Gaensicke, B. & Marsh, T. (eds.) *20th European White Dwarf Workshop*, vol. 509 of *Astronomical Society of the Pacific Conference Series*, 255 (2017). [1611.02579](https://doi.org/10.1117/1.4961257).
17. Zenati, Y., Toonen, S. & Perets, H. B. Formation and evolution of hybrid He-CO white dwarfs and their properties. *Mon. Not. R. Astron. Soc.* **482**, 1135–1142, DOI: [10.1093/mnras/sty2723](https://doi.org/10.1093/mnras/sty2723) (2019). [1803.04444](https://doi.org/10.1093/mnras/sty2723).
18. Córscico, A. H., Althaus, L. G., Miller Bertolami, M. M. & Kepler, S. O. Pulsating white dwarfs: new insights. *Astron. Astrophys. Rev.* **27**, 7, DOI: [10.1007/s00159-019-0118-4](https://doi.org/10.1007/s00159-019-0118-4) (2019). [1907.00115](https://doi.org/10.1007/s00159-019-0118-4).
19. Córscico, A. H. & Althaus, L. G. Pulsating low-mass white dwarfs in the frame of new evolutionary sequences. I. Adiabatic properties. *Astron. Astrophys.* **569**, A106, DOI: [10.1051/0004-6361/201424352](https://doi.org/10.1051/0004-6361/201424352) (2014). [1408.6708](https://doi.org/10.1051/0004-6361/201424352).
20. Bell, K. J. *et al.* Pruning The ELM Survey: Characterizing Candidate Low-mass White Dwarfs through Photometric Variability. *Astrophys. J.* **835**, 180, DOI: [10.3847/1538-4357/835/2/180](https://doi.org/10.3847/1538-4357/835/2/180) (2017). [1612.06390](https://doi.org/10.3847/1538-4357/835/2/180).
21. Pyrzas, S. *et al.* Discovery of ZZ Ceti in detached white dwarf plus main-sequence binaries. *Mon. Not. R. Astron. Soc.* **447**, 691–697, DOI: [10.1093/mnras/stu2412](https://doi.org/10.1093/mnras/stu2412) (2015). [1411.5045](https://doi.org/10.1093/mnras/stu2412).
22. Hermes, J. J. *et al.* Insights into internal effects of common-envelope evolution using the extended Kepler mission. *Mon. Not. R. Astron. Soc.* **451**, 1701–1712, DOI: [10.1093/mnras/stv1053](https://doi.org/10.1093/mnras/stv1053) (2015). [1505.01848](https://doi.org/10.1093/mnras/stv1053).
23. Hallakoun, N. *et al.* SDSS J1152+0248: an eclipsing double white dwarf from the Kepler K2 campaign. *Mon. Not. R. Astron. Soc.* **458**, 845–854, DOI: [10.1093/mnras/stw364](https://doi.org/10.1093/mnras/stw364) (2016). [1507.06311](https://doi.org/10.1093/mnras/stw364).
24. Vernet, J. *et al.* X-shooter, the new wide band intermediate resolution spectrograph at the ESO Very Large Telescope. *Astron. Astrophys.* **536**, A105, DOI: [10.1051/0004-6361/201117752](https://doi.org/10.1051/0004-6361/201117752) (2011). [1110.1944](https://doi.org/10.1051/0004-6361/201117752).
25. Dhillon, V. *et al.* First light with HiPERCAM on the GTC. In *Ground-based and Airborne Instrumentation for Astronomy VII*, vol. 10702 of *Society of Photo-Optical Instrumentation Engineers (SPIE) Conference Series*, 107020L, DOI: [10.1117/12.2312041](https://doi.org/10.1117/12.2312041) (2018). [1807.00557](https://doi.org/10.1117/12.2312041).
26. Gaia Collaboration *et al.* Gaia Data Release 2. Summary of the contents and survey properties. *Astron. Astrophys.* **616**, A1, DOI: [10.1051/0004-6361/201833051](https://doi.org/10.1051/0004-6361/201833051) (2018). [1804.09365](https://doi.org/10.1051/0004-6361/201833051).
27. Bailer-Jones, C. A. L., Rybizki, J., Fouesneau, M., Mantelet, G. & Andrae, R. Estimating Distance from Parallaxes. IV. Distances to 1.33 Billion Stars in Gaia Data Release 2. *Astron. J.* **156**, 58, DOI: [10.3847/1538-3881/aacb21](https://doi.org/10.3847/1538-3881/aacb21) (2018). [1804.10121](https://doi.org/10.3847/1538-3881/aacb21).
28. Copperwheat, C. M. *et al.* Physical properties of IP Pegasi: an eclipsing dwarf nova with an unusually cool white dwarf. *Mon. Not. R. Astron. Soc.* **402**, 1824–1840, DOI: [10.1111/j.1365-2966.2009.16010.x](https://doi.org/10.1111/j.1365-2966.2009.16010.x) (2010). [0911.1637](https://doi.org/10.1111/j.1365-2966.2009.16010.x).
29. Rasmussen, C. E. & Williams, C. K. I. *Gaussian Processes for Machine Learning* (The MIT Press, 2006).
30. Koester, D. White dwarf spectra and atmosphere models. *Memorie della Soc. Astron. Italiana* **81**, 921–931 (2010).
31. Scargle, J. D. Studies in astronomical time series analysis. II. Statistical aspects of spectral analysis of unevenly spaced data. *Astrophys. J.* **263**, 835–853, DOI: [10.1086/160554](https://doi.org/10.1086/160554) (1982).
32. Kilic, M. *et al.* A refined search for pulsations in white dwarf companions to millisecond pulsars. *Mon. Not. R. Astron. Soc.* **479**, 1267–1272, DOI: [10.1093/mnras/sty1546](https://doi.org/10.1093/mnras/sty1546) (2018). [1806.03650](https://doi.org/10.1093/mnras/sty1546).
33. Istrate, A. G. *et al.* Models of low-mass helium white dwarfs including gravitational settling, thermal and chemical diffusion, and rotational mixing. *Astron. Astrophys.* **595**, A35, DOI: [10.1051/0004-6361/201628874](https://doi.org/10.1051/0004-6361/201628874) (2016). [1606.04947](https://doi.org/10.1051/0004-6361/201628874).
34. Panei, J. A., Althaus, L. G., Chen, X. & Han, Z. Full evolution of low-mass white dwarfs with helium and oxygen cores. *Mon. Not. R. Astron. Soc.* **382**, 779–792, DOI: [10.1111/j.1365-2966.2007.12400.x](https://doi.org/10.1111/j.1365-2966.2007.12400.x) (2007).
35. Fontaine, G., Brassard, P. & Bergeron, P. The Potential of White Dwarf Cosmochronology. *Publ. Astron. Soc. Pac.* **113**, 409–435, DOI: [10.1086/319535](https://doi.org/10.1086/319535) (2001).

36. Marsh, T. R., Dhillon, V. S. & Duck, S. R. Low-Mass White Dwarfs Need Friends - Five New Double-Degenerate Close Binary Stars. *Mon. Not. R. Astron. Soc.* **275**, 828, DOI: [10.1093/mnras/275.3.828](https://doi.org/10.1093/mnras/275.3.828) (1995).
37. Bours, M. C. P. *et al.* Precise parameters for both white dwarfs in the eclipsing binary CSS 41177. *Mon. Not. R. Astron. Soc.* **438**, 3399–3408, DOI: [10.1093/mnras/stt2453](https://doi.org/10.1093/mnras/stt2453) (2014). [1401.1503](https://arxiv.org/abs/1401.1503).
38. Bours, M. C. P., Marsh, T. R., Gänsicke, B. T. & Parsons, S. G. HST+COS spectra of the double white dwarf CSS 41177 place the secondary inside the pulsational instability strip. *Mon. Not. R. Astron. Soc.* **448**, 601–605, DOI: [10.1093/mnras/stv021](https://doi.org/10.1093/mnras/stv021) (2015). [1501.04628](https://arxiv.org/abs/1501.04628).
39. Prada Moroni, P. G. & Straniero, O. Very low-mass white dwarfs with a C-O core. *Astron. Astrophys.* **507**, 1575–1583, DOI: [10.1051/0004-6361/200912847](https://doi.org/10.1051/0004-6361/200912847) (2009). [0909.2742](https://arxiv.org/abs/0909.2742).
40. Han, Z., Tout, C. A. & Eggleton, P. P. Low- and intermediate-mass close binary evolution and the initial-final mass relation. *Mon. Not. R. Astron. Soc.* **319**, 215–222, DOI: [10.1046/j.1365-8711.2000.03839.x](https://doi.org/10.1046/j.1365-8711.2000.03839.x) (2000). [astro-ph/0010269](https://arxiv.org/abs/astro-ph/0010269).
41. Tremblay, P. E., Kalirai, J. S., Soderblom, D. R., Cignoni, M. & Cummings, J. White Dwarf Cosmochronology in the Solar Neighborhood. *Astrophys. J.* **791**, 92, DOI: [10.1088/0004-637X/791/2/92](https://doi.org/10.1088/0004-637X/791/2/92) (2014). [1406.5173](https://arxiv.org/abs/1406.5173).
42. Press, W. H., Teukolsky, A. A., Vetterling, W. T. & Flannery, B. P. *Numerical recipes. The art of scientific computing, 3rd edn.* (Cambridge: University Press, 2007).
43. Foreman-Mackey, D., Hogg, D. W., Lang, D. & Goodman, J. emcee: The MCMC Hammer. *Publ. Astron. Soc. Pac.* **125**, 306, DOI: [10.1086/670067](https://doi.org/10.1086/670067) (2013). [1202.3665](https://arxiv.org/abs/1202.3665).
44. Holberg, J. B. & Bergeron, P. Calibration of Synthetic Photometry Using DA White Dwarfs. *Astron. J.* **132**, 1221–1233, DOI: [10.1086/505938](https://doi.org/10.1086/505938) (2006).
45. Tremblay, P. E., Bergeron, P. & Gianninas, A. An Improved Spectroscopic Analysis of DA White Dwarfs from the Sloan Digital Sky Survey Data Release 4. *Astrophys. J.* **730**, 128, DOI: [10.1088/0004-637X/730/2/128](https://doi.org/10.1088/0004-637X/730/2/128) (2011). [1102.0056](https://arxiv.org/abs/1102.0056).
46. Claret, A. Non-linear limb-darkening law for LTE models (Claret, 2000). *VizieR Online Data Catalog* **336**, 31081 (2000).
47. Gianninas, A., Strickland, B. D., Kilic, M. & Bergeron, P. Limb-darkening Coefficients for Eclipsing White Dwarfs. *Astrophys. J.* **766**, 3, DOI: [10.1088/0004-637X/766/1/3](https://doi.org/10.1088/0004-637X/766/1/3) (2013). [1301.7091](https://arxiv.org/abs/1301.7091).
48. Foreman-Mackey, D., Agol, E., Ambikasaran, S. & Angus, R. Fast and Scalable Gaussian Process Modeling with Applications to Astronomical Time Series. *Astron. J.* **154**, 220, DOI: [10.3847/1538-3881/aa9332](https://doi.org/10.3847/1538-3881/aa9332) (2017). [1703.09710](https://arxiv.org/abs/1703.09710).
49. Schlafly, E. F. & Finkbeiner, D. P. Measuring Reddening with Sloan Digital Sky Survey Stellar Spectra and Recalibrating SFD. *Astrophys. J.* **737**, 103, DOI: [10.1088/0004-637X/737/2/103](https://doi.org/10.1088/0004-637X/737/2/103) (2011). [1012.4804](https://arxiv.org/abs/1012.4804).
50. Lenz, P. & Breger, M. Period04 User Guide. *Commun. Asteroseismol.* **146**, 53–136, DOI: [10.1553/cia146s53](https://doi.org/10.1553/cia146s53) (2005).
51. Hermes, J. J. *et al.* White Dwarf Rotation as a Function of Mass and a Dichotomy of Mode Line Widths: Kepler Observations of 27 Pulsating DA White Dwarfs through K2 Campaign 8. *Astrophys. J. Suppl.* **232**, 23, DOI: [10.3847/1538-4365/aa8bb5](https://doi.org/10.3847/1538-4365/aa8bb5) (2017). [1709.07004](https://arxiv.org/abs/1709.07004).

Correspondence and requests for materials should be addressed to Dr. S. G. Parsons (s.g.parsons@sheffield.ac.uk)

Acknowledgements

S.G.P. acknowledges the support of a Science and Technology Facilities Council (STFC) Ernest Rutherford Fellowship. HiPERCAM and V.S.D. are funded by the European Research Council under the European Union’s Seventh Framework Programme (FP/2007-2013) under ERC-2013-ADG Grant Agreement no. 340040 (HiPERCAM). Partial support for this work was provided by NASA K2 Cycle 6 Grant 80NSSC19K0162. A.G.I acknowledges support from the Netherlands Organisation for Scientific Research (NWO).

Based on observations made with the Gran Telescopio Canarias (programme ID GTC59-18B), installed in the Spanish Observatorio del Roque de los Muchachos of the Instituto de Astrofísica de Canarias, in the island of La Palma. Based on observations made with ESO Telescopes at the La Silla Paranal Observatory under programme ID 097.D-0786.

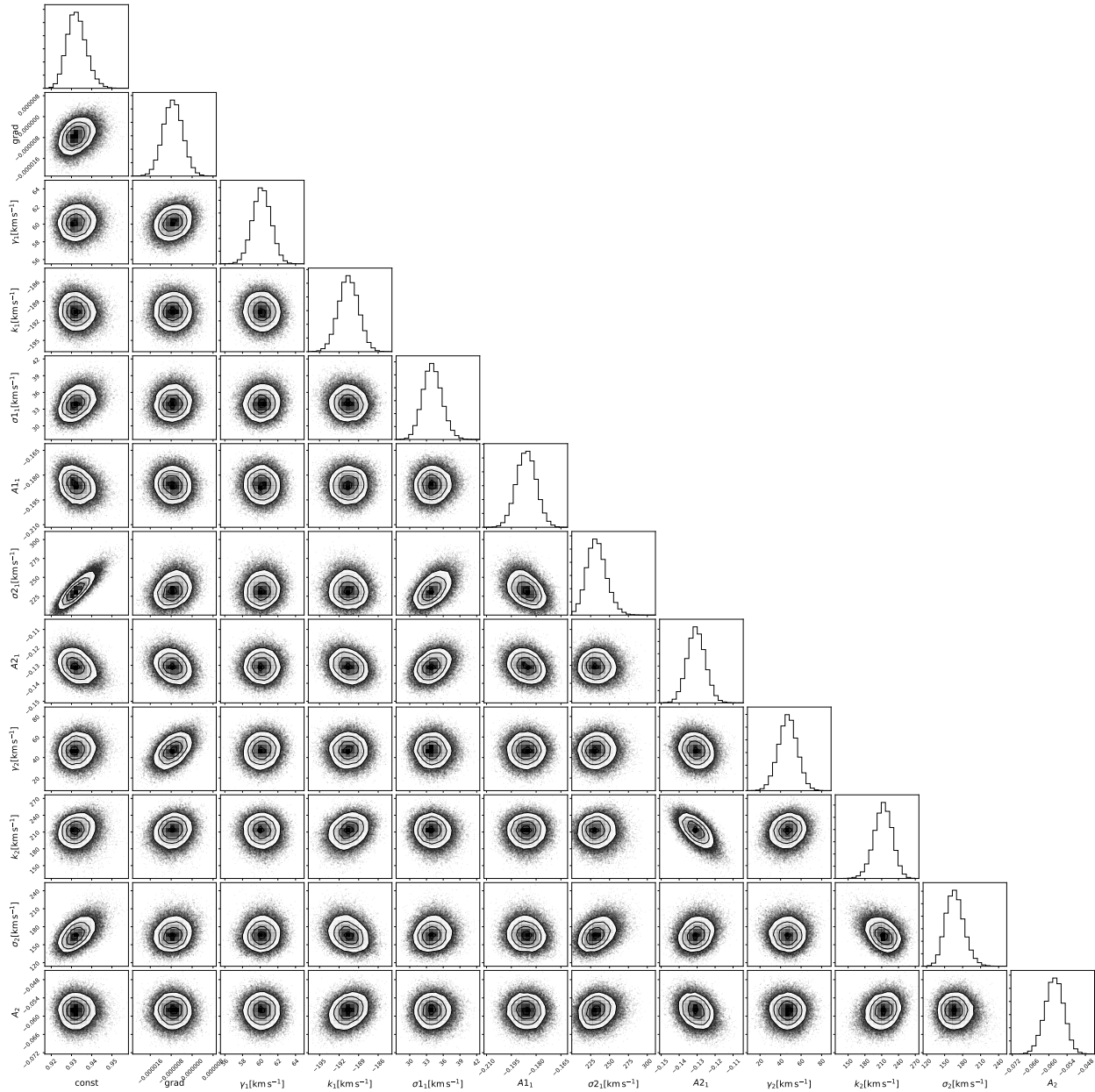
Author contributions statement

All authors have contributed to the work presented in this paper. S.G.P. reduced all the spectroscopic and photometric data and carried out the SED fitting. S.G.P. and V.S.D. performed the GTC observations. A.J.B. performed the radial velocity and light curve fitting. S.P.L. wrote the Python code that implemented Gaussian Processes in the light curve fitting. V.S.D., S.P.L.,

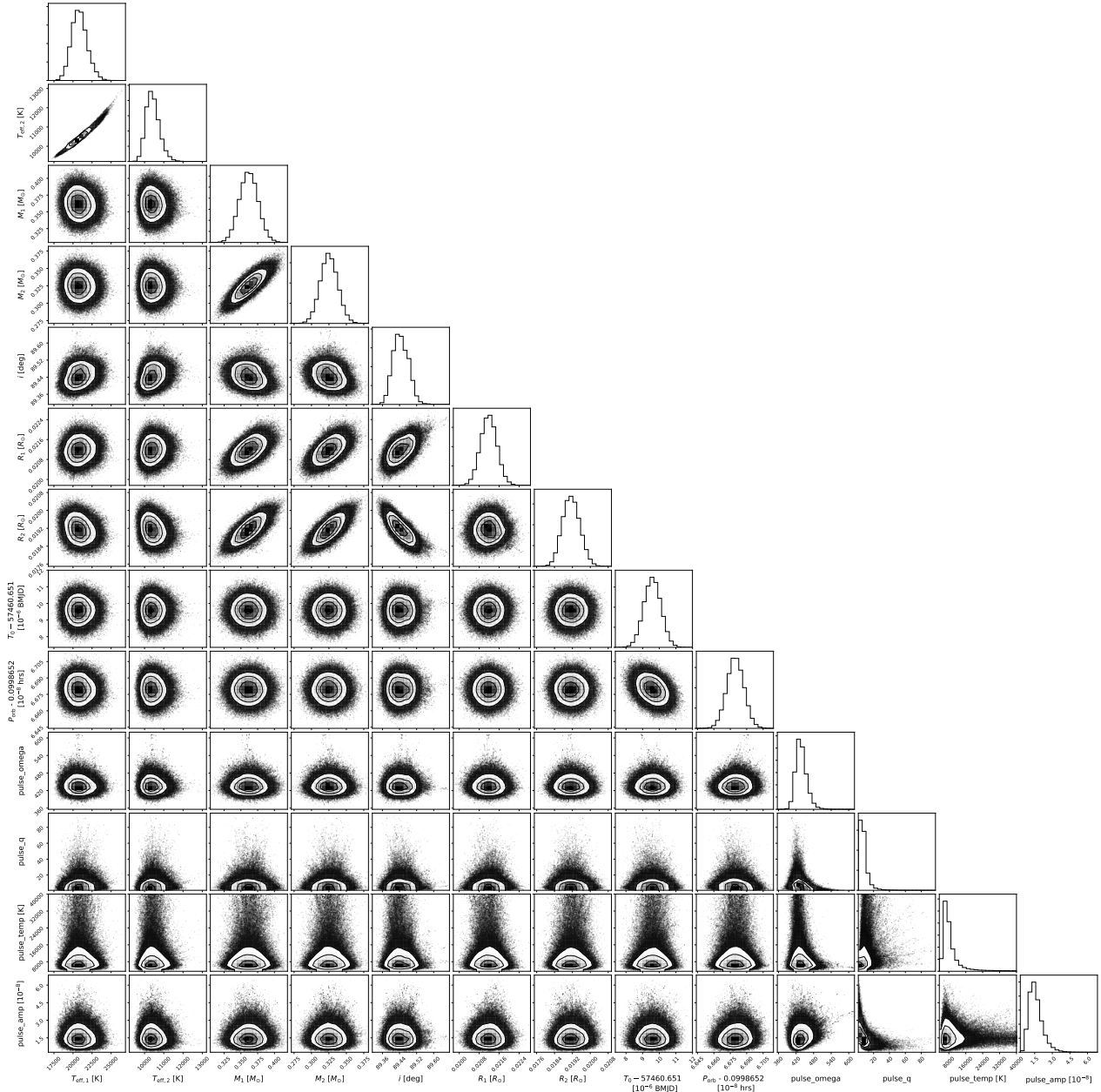
T.R.M., S.G.P., E.B. M.J.D., M.J.G. and D.I.S. all contributed to the development and support of HiPERCAM. J.J.H. analysed the pulsations in the HiPERCAM light curves. A.G.I. investigated the internal structure of the white dwarfs and the evolution of the binary. All authors reviewed the manuscript.

Additional information

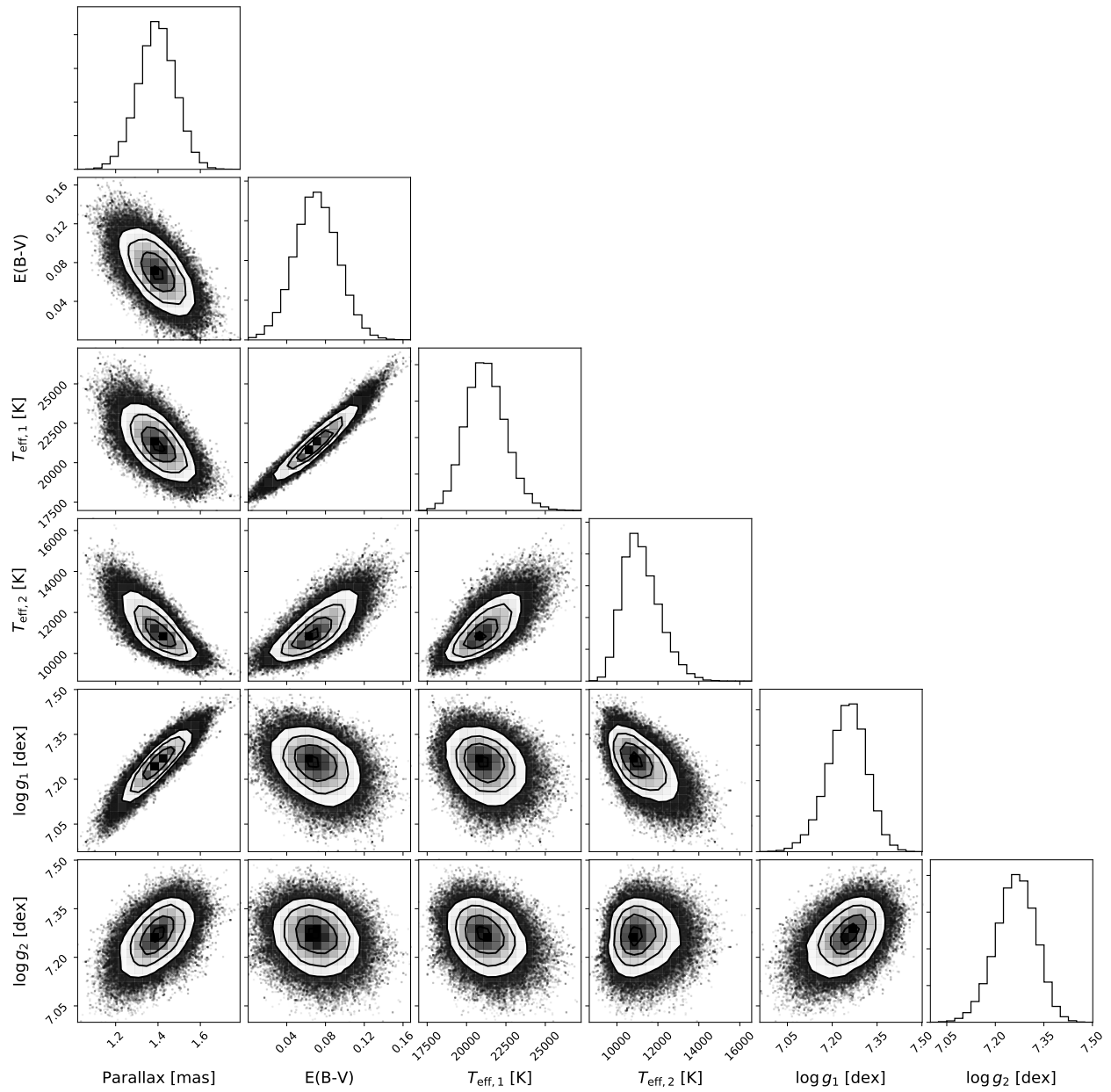
Competing Interests. The authors declare that they have no competing financial interests.



Supplementary Figure 1. Posterior probability distributions for model parameters obtained through fitting the $H\alpha$ absorption lines of both white dwarfs. Grey-scalers and contours represent the joint probability distributions for each pair of parameters, while the histograms show the marginalised probability distributions for each parameter.



Supplementary Figure 2. Posterior probability distributions for model parameters obtained through fitting the multi-band HiPERCAM light curves.



Supplementary Figure 3. Posterior probability distributions for model parameters obtained from the spectral energy distribution fit.